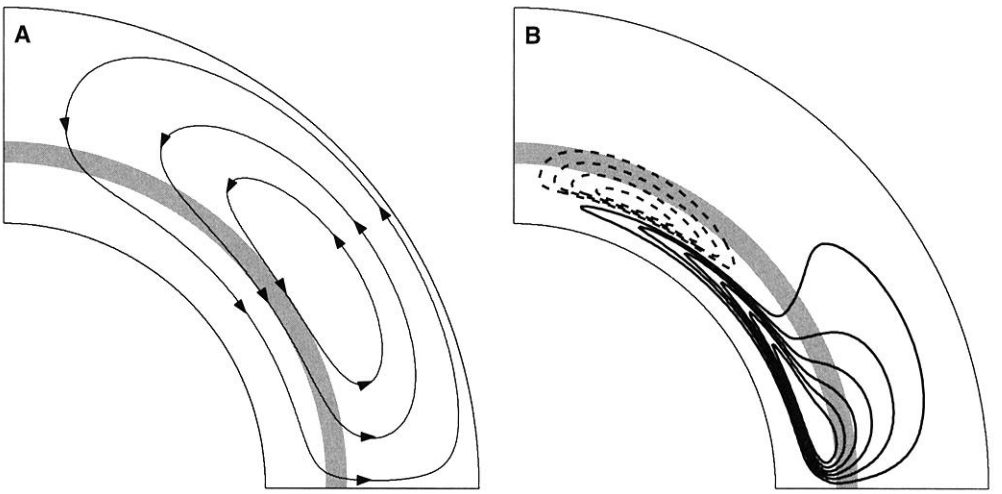

Fig. 3. A meridional cut of the Sun corresponding to the simulation geometry (the same domain as in Fig. 1). The meridional circulation (**A**) is depicted by black streamlines with arrows marking the direction of flow. The flow now penetrates below the tachocline (the shaded gray region) down to a depth of 0.6*R*. A snapshot of the toroidal field configuration at a particular instant of time (**B**) shows a belt of negative toroidal field (dashed contours) being pushed below the tachocline (into the stable region) by the penetrating flow at high latitudes, while simultaneously at low latitudes, a belt of positive toroidal field (solid contours) is being pushed out into the convection zone, where it can erupt to form sunspots.

mechanism can drive such a deeply penetrating meridional flow. However, recent simulations of solar convection show that downward-directed convective plumes (originating in the SCZ and penetrating into the stable regions below) tend to have a net equatorward motion inside the stable region (*27, 28*). These downward plumes are capable of pushing the magnetic field into the stable interior (*29*).

We have shown that a meridional circulation penetrating below the tachocline can explain the latitudinal distribution of sunspots. At present, this seems the best way to resolve the impasse that has been plaguing modern solar dynamo theory. Although the ill-understood question of angular momentum balance (*30*) must be addressed for a flow penetrating into the nearly uniformly rotating upper radiative region, this flow would help in explaining the lithium depletion and its connection to angular momentum loss (*31*) observed in stars at various phases of stellar evolution. A penetrating flow can also contribute to the sound speed anomaly that is observed beneath the tachocline (*32, 33*).

References and Notes

1. S. H. Schwabe, *Astron. Nachr.* **21**, 2 (1844).
2. G. E. Hale, *Astrophys. J.* **28**, 315 (1908).
3. E. N. Parker, *Astrophys. J.* **122**, 293 (1955).
4. ———, *Cosmical Magnetic Fields* (Clarendon, Oxford, 1979).
5. A. R. Choudhuri, *The Physics of Fluids and Plasmas: An Introduction for Astrophysicists* (Cambridge Univ. Press, Cambridge, 1998).
6. J. Schou *et al.*, *Astrophys. J.* **505**, 390 (1998).
7. P. Charbonneau *et al.*, *Astrophys. J.* **527**, 445 (1999).
8. A. R. Choudhuri, P. A. Gilman, *Astrophys. J.* **316**, 788 (1987).
9. S. D'Silva, A. R. Choudhuri, *Astron. Astrophys.* **272**, 621 (1993).
10. Y. Fan, G. H. Fisher, E. E. DeLuca, *Astrophys. J.* **405**, 390 (1993).
11. H. W. Babcock, *Astrophys. J.* **133**, 572 (1961).
12. R. B. Leighton, *Astrophys. J.* **156**, 1 (1969).
13. A. R. Choudhuri, M. Schüssler, M. Dikpati, *Astron. Astrophys.* **303**, L29 (1995).
14. M. Dikpati, P. Charbonneau, *Astrophys. J.* **518**, 508 (1999).
15. M. Küker, G. Rüdiger, M. Schultz, *Astron. Astrophys.* **374**, 301 (2001).
16. D. Nandy, A. R. Choudhuri, *Astrophys. J.* **551**, 576 (2001).
17. Y.-M. Wang, N. R. Sheeley, A. G. Nash, *Astrophys. J.* **383**, 431 (1991).
18. B. R. Durney, *Sol. Phys.* **160**, 213 (1995).
19. ———, *Astrophys. J.* **486**, 1065 (1997).
20. P. M. Giles, T. L. Duvall, P. H. Scherrer, R. S. Bogart, *Nature* **390**, 52 (1997).
21. D. C. Braun, Y. Fan, *Astrophys. J.* **508**, L105 (1998).
22. Methods are available as supporting material on *Science* Online.
23. J. A. Markiel, J. H. Thomas, *Astrophys. J.* **523**, 827 (1999).
24. D. Nandy, A. R. Choudhuri, in preparation.
25. E. A. Spiegel, N. O. Weiss, *Nature* **287**, 616 (1980).
26. A. A. Van Ballegooijen, *Astron. Astrophys.* **113**, 99 (1982).
27. N. H. Brummell, N. E. Hurlburt, J. Toomre, *Astrophys. J.* **493**, 955 (1998).
28. M. S. Miesch *et al.*, *Astrophys. J.* **532**, 593 (2000).
29. S. M. Tobias, N. H. Brummell, T. L. Clune, J. Toomre, *Astrophys. J.* **549**, 1183 (2001).
30. B. R. Durney, *Astrophys. J.* **528**, 486 (2000).
31. J.-P. Zahn, *Astron. Astrophys.* **265**, 115 (1992).
32. A. G. Kosovichev *et al.*, *Sol. Phys.* **170**, 43 (1997).
33. J. R. Elliot, D. O. Gough, *Astrophys. J.* **516**, 475 (1999).

34. We thank B. Durney, M. Miesch, A. Kosovichev, P. Scherrer, and H. M. Antia for critical discussions on various aspects of the present study.

Supporting Online Material

www.sciencemag.org/cgi/content/full/296/5573/1671/DC1

Methods

15 February 2002; accepted 17 April 2002

Biodegradable, Elastic Shape-Memory Polymers for Potential Biomedical Applications

Andreas Lendlein[1]* and Robert Langer[2]

The introduction of biodegradable implant materials as well as minimally invasive surgical procedures in medicine has substantially improved health care within the past few decades. This report describes a group of degradable thermoplastic polymers that are able to change their shape after an increase in temperature. Their shape-memory capability enables bulky implants to be placed in the body through small incisions or to perform complex mechanical deformations automatically. A smart degradable suture was created to illustrate the potential of these shape-memory thermoplastics in biomedical applications.

Current approaches for implanting medical devices, many of which are polymeric in nature, often require complex surgery followed by device implantation. With the advent of minimally invasive surgery (*1*), it is possible to place small devices with laprascopes. Such advances create new opportunities but also new challenges. How does one implant a bulky device or knot a suture in a confined space? It occurred to us that the creation of biocompatible (and ideally in many cases degradable) shape-memory polymers with the appropriate mechanical properties might enable the development of novel types of medical devices.

Shape-memory polymers possess the ability to memorize a permanent shape that can substantially differ from their initial temporary shape. Large bulky devices could thus potential-

[1]mnemoScience GmbH, Pauwelsstraße 19, D-52074 Aachen, and Institute for Technical and Macromolecular Chemistry, RWTH Aachen, Germany. [2]Department of Chemical Engineering, Massachusetts Institute of Technology, 45 Carleton Street, Cambridge, MA 02139, USA.

*To whom correspondence should be addressed. E-mail: a.lendlein@mnemoscience.de

ly be introduced into the body in a compressed temporary shape by means of minimally invasive surgery and then be expanded on demand to their permanent shape to fit as required. In the same way, a complex mechanical deformation could be performed automatically instead of manually by the surgeon. The transition from the temporary to the permanent shape could be initiated by an external stimulus such as a temperature increase above the switching transition temperature T_{trans} of the polymer [movie S1 (*19*)].

The thermally induced shape-memory effect has been described for different material classes: polymers (*2*, *3*), such as polyurethanes (*4*–*7*), poly(styrene-*block*-butadiene) (*8*) and polynorbornene (*9*, *10*); hydrogels (*11*, *12*); metallic alloys (*13*); and ceramics (*14*). All of these materials are nondegradable in physiological environments and many lack either biocompatibility or compliance in mechanical properties.

In metallic alloys, the shape-memory effect is due to a martensitic phase transition (*13*). In contrast, the polymers designed to exhibit a thermally induced shape-memory effect require two components on the molecular level: cross-links to determine the permanent shape and switching segments with T_{trans} to fix the temporary shape. Above T_{trans}, the permanent shape can be deformed by application of an external stress. After cooling below T_{trans} and subsequent release of the external stress, the temporary shape is obtained. The sample recovers its permanent shape upon heating to $T > T_{trans}$.

Cross-links can be either covalent bonds or physical interactions. Recently, we have reported on shape-memory polymers (*15*), which are covalently cross-linked polymer networks containing hydrolyzable switching segments. Emphasis in the present work was put on the development of a group of polymers that contain physical cross-links. These thermoplastics are easily processed from solution or melt and are substantially tougher than polymer networks. In particular, they are degradable, showing linear mass loss during hydrolytic degradation.

We selected linear, phase-segregated multiblockcopolymers as the structural concept for our polymer system, because this polymer architecture allows tailoring of macroscopic properties by variation of molecular parameters.

In the first step of the polymer synthesis, macrodiols with different thermal characteristics are synthesized through ring-opening polymerization of cyclic diesters or lactones, with a low-molecular-weight diol as initiator, and purified (*16*). In the current study, oligo(ε-caprolactone)diol (OCL) was chosen as the precursor for the switching segments having a melting transition temperature (T_m). Crystallizable oligo(*p*-dioxanone)diol (ODX), with a higher T_m than OCL was chosen as a hard segment to provide the physical cross-links (*17*). The melting transition of the latter macrodiols is determined by the average chain length, which can be tailored by the monomer/initiator ratio (*16*, *17*).

In the second step, the two macrodiols are coupled with 2,2(4),4-trimethylhexanediisocya-

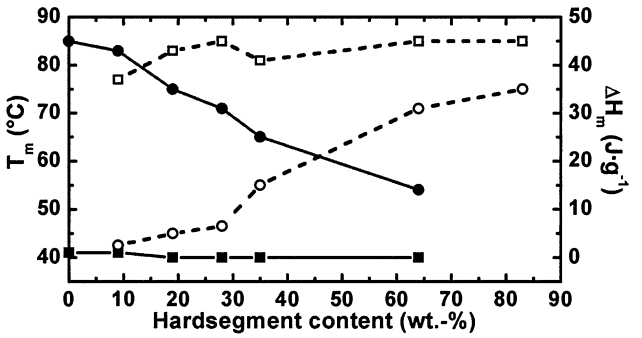

Fig. 1. T_m and enthalpies ΔH_m of multiblockcopolymers (*36*). T_m (OCL), solid squares; ΔH_m (OCL), solid circles; T_m (ODX), open squares; ΔH_m (ODX), open circles.

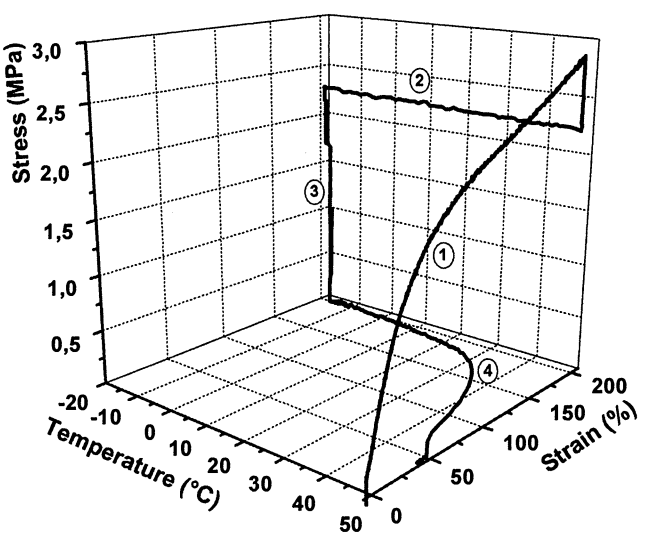

Fig. 2. Cyclic thermomechanical experiment of PDC35 (*37*) with T_{trans} = 40°C. Results of the first cycle are shown. Step 1 of the experiment was strain-controlled; steps 2 through 4 to the beginning of next cycle were stress-controlled.

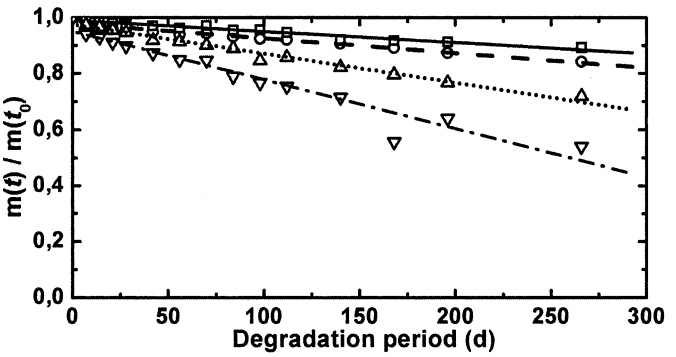

Fig. 3. Hydrolytic degradation of thermoplastic shape-memory elastomers in aqueous buffer solution (pH 7) at 37°C. The relative mass loss for multiblockcopolymers differing in their hard segment content is shown (PDC10, circles; PDC17, squares; PDC31, upward-pointing triangles; PDC42, downward-pointing triangles). m(*t*), Sample mass after a degradation period *t*; m(t_0), original sample mass.

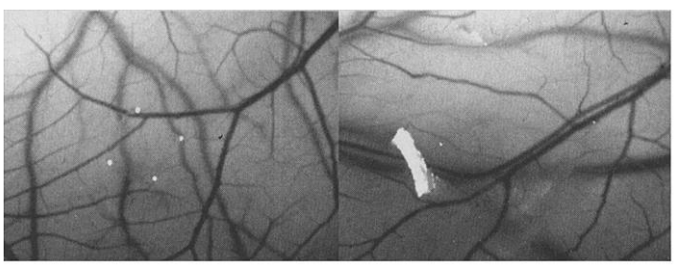

Fig. 4. Results of CAM tests of PDC38 (sample length: left, ~0.3 cm; right, ~0.5 cm). For a positive control sample, see (*25*).

nate (*18*). Hard segment contents of the synthesized polymers range from 0 to 83 weight % (wt %); and number-average molecular weights (M_n), which were determined by means of gel permeation chromatography relative to polystyrene standards, are between 35,000 and 77,000, with polydispersities around 2. Figure 1 shows melting properties of multiblockcopolymers differing in their hard segment contents. Glass transition temperatures are between –51° and 0°C [table S2 (*19*)].

The multiblockcopolymers can be elongated up to 1000% [table S1 (*19*)] before they break. This allows deformations between permanent and temporary shape up to 400%, whereas the maximum deformation for Ni-Ti alloys is 8% (*20*). The mechanical properties strongly depend on the hard segment content. Increasing the amount of ODX in the reaction mixture leads to a stiffer polymer and a decrease of the corresponding elongations at break. This can be observed at all three investigated temperatures and is due to increased crystallinity [table S1 (*19*)].

To quantify shape-memory properties, programming and recovery were investigated by cyclic thermomechanical tests (*21*, *22*). This simple test describes shape memory in one dimension; however, the effect takes place in all three dimensions. The effect is commonly described with two important parameters. The strain fixity rate R_f describes the ability of the switching segment to fix the mechanical deformation, which is applied during the programming process. For our polymers, R_f lies between 98 and 99.5%. The strain recovery rate R_r quantifies the ability of the material to recover its permanent shape. R_r depends on the cycle number and gradually approaches 100% because of reorientation of the polymer chains in the unoriented pressed films during the early cycles, because of inelastic behavior. In the first cycle, R_r has values between 76 and 80% for our multiblockcopolymers and reaches 98 to 99% in the third cycle. Ni-Ti alloys show stresses in the range of 200 to 400 MPa during shape-memory transition, whereas the shape-memory thermoplastics produce stresses in the range between 1 and 3 MPa, depending on the hard segment content (*23*). The lower value for shape-memory polymers resembles the mechanical stresses in soft tissue (*24*).

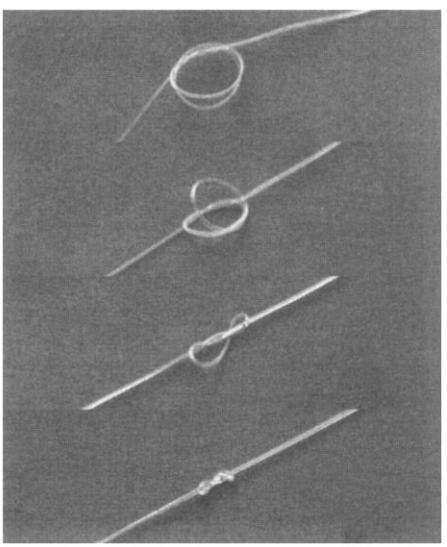

Fig. 5. A fiber of a thermoplastic shape-memory polymer was programmed by stretching about 200%. After forming a loose knot, both ends of the suture were fixed. The photo series shows, from top to bottom, how the knot tightened in 20 s when heated to 40°C. This experiment is also available as movie S2 (*19*).

To record the change in elongation during the shape-memory effect, another cyclic thermomechanical experiment was performed (Fig. 2). Step 1 is the deformation of the permanent shape and corresponds to a standard stress-strain test. After maintaining this strain for 5 min to allow relaxation for chains, the stress is then held constant while the sample is cooled (step 2), whereby the temporary shape is fixed. Then stress is completely removed after waiting for 10 min (step 3), and the sample is now in its temporary shape. Heating in step 4 (2 K min^{-1}) actuates the shape-memory effect. The contraction of the sample can be observed on the strain axis, and the fastest shape change is recorded at T_{trans} = 40°C.

We introduced hydrolyzable ester bonds in our polymers so that they would cleave under physiological conditions. The degradation kinetics can be controlled through the composition and relative mass content of the precursor macrodiols. An increase in the ODX content leads to a faster loss in mass (Fig. 3), because the concentration of rapidly hydrolyzable ODX-ester bonds in the amorphous phase is increased.

Established synthetic degradable suture materials are mainly aliphatic polyhydroxy acids showing bulk degradation. This degradation process can be split into several stages (*25*), the first three of which are swelling, loss of molecular weight, and loss of sample mass.

The degradation of L-lactide–based polyesters shows a nonlinear mass loss leading to a sudden release of potentially acidic degradation products from the bulk material, which may cause a strong inflammatory response (*26*). The high crystallinity of oligomer particles slows down degradation at the end of the process and leads to the formation of fibrous capsules in vivo (*27*). In contrast, the multiblockcopolymers presented here show linear mass loss in vitro (Fig. 3), resulting in a continuous release of degradation products.

The tissue compatibility of our polymer was investigated with chorioallantoic membrane (CAM) tests, which are a sensitive method of evaluating toxicity (*28*). Nine separate experiments were carried out. All tests showed good tissue compatibility when graded according to Folkman (*29*). There was no detectable change in the number or shape of blood vessels or damage under or in the vicinity of the polymer film (Fig. 4).

A challenge in endoscopic surgery is the tying of a knot with instruments and sutures to close an incision or open lumen. It is especially difficult to manipulate the suture so that the wound lips are pressed together under the right stress. When the knot is fixed with a force that is too strong, necrosis of the surrounding tissue can occur (*30*). If the force is too weak, scar tissue, which has poorer mechanical properties, forms and may lead to the formation of hernias (*31*). A possible solution is the design of a smart surgical suture, whose temporary shape would be obtained by elongating the fiber with controlled stress. This suture could be applied loosely in its temporary shape; when the temperature was raised above T_{trans}, the suture would shrink and tighten the knot, applying the optimum force (*32*) (Fig. 5).

An additional set of experiments to test the feasibility of this concept was performed. The highly elastic shape-memory thermoplastics were extruded into monofilaments (*33*). A sterilized suture (*34*) was programmed under sterile conditions by exerting a controlled stress on the extruded fiber and subsequent thermal quenching. This smart suture was tested in the following animal model: A rat (WAG; weight, 250 g; albino) was killed and shaved. An incision was made through the belly tissue and the abdominal muscle. The wound was loosely sutured with a standard surgical needle (Hermann Butsch, size 15, ⅜ circle). When the temperature was increased to 41°C, the shape-memory effect was actuated (Fig. 6). This test was carried out four times using two different animals. For these tests, the fibers were elongated by 200% during programming and were able to generate a force of 1.6 N upon actuation of the shape-memory effect in vitro. During the animal experiment, 0.1 N could be detected in the surrounding tissue (*35*).

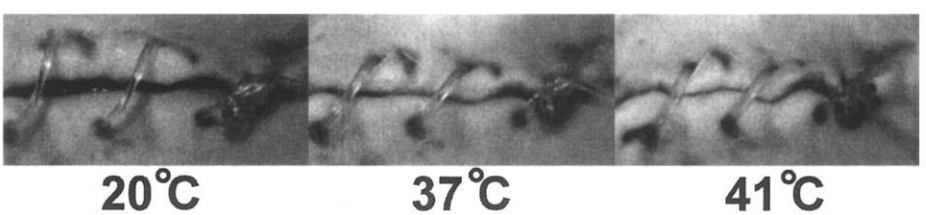

Fig. 6. Degradable shape-memory suture for wound closure. The photo series from the animal experiment shows (left to right) the shrinkage of the fiber while temperature increases.

This feasibility study suggests that this type of material has the potential to influence how implants are designed and could enable new surgical devices in the future.

References and Notes

1. J. G. Hunter, Ed., *Minimally Invasive Surgery* (McGraw-Hill, New York, 1993).
2. A. Charlesby, *Atomic Radiation and Polymers* (Pergamon, Oxford, 1960), pp. 198–257.
3. Y. Kagami, J. P. Gong, Y. Osada, *Macromol. Rapid Commun.* **17**, 539 (1996).
4. B. K. Kim, S. Y. Lee, M. Xu, *Polymer* **37**, 5781 (1996).
5. J. R. Lin, L. W. Chen, *J. Appl. Polym. Sci.* **69**, 1563 (1998).
6. ———, *J. Appl. Polym. Sci.* **69**, 1575 (1998).
7. T. Takahashi, N. Hayashi, S. Hayashi, *J. Appl. Polym. Sci.* **60**, 1061 (1996).
8. K. Sakurai, Y. Shirakawa, T. Kahiwagi, T. Takahashi, *Polymer* **35**, 4238 (1994).
9. K. Sakurai, T. Takahashi, *J. Appl. Polym. Sci.* **38**, 1191 (1989).
10. K. Sakurai, T. Kashiwagi, T. Takahashi, *J. Appl. Polym. Sci.* **47**, 937 (1993).
11. Y. Osada, A. Matsuda, *Nature* **376**, 219 (1995).
12. Z. Hu, X. Zhang, Y. Li, *Science* **269**, 525 (1995).
13. L. M. Schetky, *Sci. Am.* **241**, 68 (November 1979).
14. M. V. Swain, *Nature* **322**, 234 (1986).
15. A. Lendlein, A. Schmidt, R. Langer, *Proc. Natl. Acad. Sci. U.S.A.* **98**, 842 (2001).
16. A. Lendlein, P. Neuenschwander, U. W. Suter, *Macromol. Chem. Phys.* **201**, 1067 (2000).
17. H. G. Grablowitz, A. Lendlein, in preparation.
18. Both macrodiols were dissolved in 1,2-dichloroethane and heated to 80°C. An equimolar amount of 2,2(4),4-trimethylhexanediisocyanate was added. The synthesis was carried out under exclusion of water, and solvents and monomers were dried by standard techniques. The crude product was precipitated in hexane.
19. Data and video are available as supporting material on *Science* Online.
20. J. Van Humbeeck, *Mater. Sci. Eng.* **A273-275**, 134 (1999).
21. The material was pressed into films having a thickness of 300 to 500 μm. Dog bone–shaped samples (length between clamps, 6 mm; width, 3 mm) were punched out of the films and mounted in a tensile tester equipped with a thermo chamber (*8*, *21*). The tests were carried out at 200% strain at a strain rate of 10 mm min^{-1} with a low temperature (T_{low}) of –20°C and a high temperature (T_{high}) of 50°C. The samples were held at T_{low} for 10 min before the load was removed.
22. H. Tobushi, H. Hara, E. Yamada, S. Hayashi, *Soc. Photo-Opt. Instrum. Eng.* **2716**, 46 (1996).
23. H. Tobushi, S. Hayashi, A. Ikai, H. Hara, *J. Physique IV* **6**, C1-377 (1996).
24. A. F. T. Mak, M. Zhang, in *Handbook of Biomaterial Properties*, J. Black, G. Hastings, Eds. (Chapman and Hall, New York, ed. 1, 1998), pp. 66–69.
25. A. Lendlein, *Chem. Unserer Zeit* **33**, 279 (1999).
26. K. Fu, D. W. Pack, A. M. Klibanov, R. S. Langer, *Pharm. Res.* **17:1**, 100 (2000).
27. K. A. Hooper, N. D. Macon, J. Kohn, *J. Biomed. Mater. Res.* **32**, 443 (1998).
28. K. Spanel-Borowski, *Res. Exp. Med. (Berlin)* **189**, 69 (1989).
29. R. Crum, S. Szabo, J. Folkman, *Science* **230**, 1375 (1985).
30. J. Hoer, U. Klinge, A. Schachtrupp, Ch. Töns, V. Schumpelick, *Langenb. Arch. Surg.* **386**, 218 (2001).
31. N. C. F. Hodgson, R. A. Malthaner, T. Østbye, *Ann. Surg.* **231**, 436 (2000).
32. Control of stress was achieved on three levels: in the material itself through hard segment content, by programming, and during application through the looseness of the loops of the suture.
33. Extrusion was at 90°C through a 1-mm rod die on a Haake Polylab single-screw extruder.
34. Sterilization was done with ethylene oxide at 45°C.
35. The force of the fiber was determined with a tensile tester equipped with a thermo chamber. The force on the surrounding tissue was estimated by mounting a spring of known stiffness close to the wound and measuring the length change.
36. T_m and enthalpies ΔH_m of multiblockcopolymers were measured on a Perkin-Elmer DSC 7 at a heating rate of 10 K min^{-1}. The results were taken from the second heating run.
37. The weight content of ODX in the polymer is given by the two-digit number in the sample ID.

38. We thank H. Grablowitz for degradation experiments, J. Schulte for mechanical tests, W. Grasser for graphics, D. Rickert and M. Moses (Children's Hospital, Boston) for CAM tests, and R.-P. Franke (Zentralinstitut für biomedizinische Technik, University of Ulm) for the animal experiment. A.L. is grateful to Fonds der Chemischen Industrie for a Liebig fellowship. Partially funded by Bundesministerium für Bildung und Forschung BioFuture award no. 0311867.

Supporting Online Material
www.sciencemag.org/cgi/content/full/1066102/DC1
Tables S1 to S3
Movies S1 and S2

10 September 2001; accepted 11 April 2002
Published online 25 April 2002;
10.1126/science.1066102
Include this information when citing this paper.

Emerging Coherence in a Population of Chemical Oscillators

István Z. Kiss, Yumei Zhai, John L. Hudson*

Coherence of interacting oscillating entities has importance in biological, chemical, and physical systems. We report experiments on populations of chemical oscillators and verify a 25-year-old theory of Kuramoto that predicts that global coupling in a set of smooth limit-cycle oscillators with different frequencies produces a phase transition in which some of the elements synchronize. Both the critical point and the predicted dependence of order on coupling are seen in the experiments. We extend the studies both to relaxation and to chaotic oscillators and characterize the quantitative similarities and differences among the types of systems.

The collective behavior and synchronization of a population of somewhat dissimilar cyclic processes depend on the dynamics of the individual elements and on the interactions among them. Wiener raised the question of collective synchronization in a discussion of alpha rhythms in the brain (*1*). Synchronization has been shown to be an important process in the persistence of species (*2*) and in the functioning of heart pacemaker cells (*3*, *4*), yeast cells (*5*), and neurons in the cat visual cortex (*6*). Visual and acoustic interactions make fireflies flash (*7*), crickets chirp (*8*), and an audience clap in synchrony (*9*). Applications in engineering may be found in coupled chemical reactions (*10*, *11*), microwave systems (*12*), lasers (*13*), and digital-logic circuitry (*14*). Winfree (*4*) and Kuramoto (*15*, *16*) made a major advance in the theory of the onset of synchronization in populations with weak global coupling. In the model, each oscillator of an infinite set is described by a single variable, the phase, and is coupled to all other elements with equal strength. The theory predicts a transition with increasing global coupling strength (K) at which some of the oscillators with originally different frequencies become coherent, and it predicts the dependence of order on K above the critical point. The theory initiated extensive theoretical activity in collective dynamics and extensions to the effects of finite-size populations (*17*), fluctuations (*18*), and more complicated waveforms and coupling mechanisms (*19*, *20*). For a recent review, see (*21*). Simulations on arrays of Josephson junctions (*14*) and of lasers (*13*) have shown that coherent motion in physical systems can be interpreted using the Kuramoto model.

In this paper, we present results of a laboratory experiment that confirm the phase transition and dependence of order on coupling strength predicted by the theory on smooth limit-cycle oscillators (*16*). We show a strong enhancement of fluctuations near the critical point that arise in finite-size systems, in accordance with the theory of Daido (*17*). In addition, we extend the experiments to relaxation and chaotic (*22*) oscillators, which often occur in physical systems. We investigate the onset of coherence and the dependence of order and finite-size fluctuations on K, and we compare the characteristics of the three types of oscillators.

The experimental system is an array of 64 nickel electrodes in sulfuric acid (fig. S1). Current, which is proportional to the rate of metal dissolution, was measured on each electrode at a constant applied potential. Periodic or chaotic oscillations were observed, depending on conditions such as applied potential, acid concentration, and added external resistance (*23*, *24*). Inherent heterogeneities on the metal surface produced a distribution of frequencies of the oscillators. K was controlled through the use of

Department of Chemical Engineering, 102 Engineers' Way, University of Virginia, Charlottesville, VA 22904-4741, USA.

*To whom correspondence should be addressed. E-mail: hudson@virginia.edu